International Journal of Concrete Structures and Materials

RESEARCH Open Access

Structural Performance of PC Double Beam–Column Connection Under Gravity and Seismic Loading

Jang-Woon Baek[1], Su-Min Kang[2*], Tae-Ho Kim[3] and Jin-Yong Kim[4]

Abstract

Recently, as a new precast concrete (PC) construction method for increasing economy and constructability, the PC double-beam system has been developed for factories or logistic centers, where construction duration is particularly important. In this study, half-scaled PC double beam–column connection was tested under gravity loading and cyclic lateral loading. The major test parameters included the use of the spliced PC column and the addition of reinforcement at the beam–column joint. In the gravity loading test, the flexural behavior of the PC double beam was investigated. The test results showed satisfactory flexural capacity at the PC double-beam section, validating the composite action between the PC and RC members. In the cyclic lateral loading test, the seismic performance of the PC double beam–column connection was investigated. Based on the test results, the failure mode, load-carrying capacity, deformation capacity, energy dissipation capacity, secant stiffness, and shear strength of the PC double-beam system were evaluated and compared with those of a conventional RC double beam–column connection. According to the test results, the structural performance of the PC double beam–column connection was comparable to that of the RC double beam–column connection and satisfied the acceptance criteria of moment frame in the ACI 374.1-05 provision.

Keywords: precast concrete double beam, precast beam–column connection, cyclic loading test, gravity loading test, precast concrete slab construction method, construction duration

1 Introduction

In recent years, various precast concrete (PC) construction methods have been developed to cope with the extensive construction demands of factories and logistics centers, where a shortening of construction duration is a particular concern for reducing the construction cost of buildings. In PC construction, the PC slab constitutes the majority of all PC members. Thus, to reduce construction costs, new PC slab construction methods have been developed. However, the concept and shape of these methods (developed in the worldwide construction markets) are similar, where the use of prestressed tendons, hollow core sections, or T-shaped sections is common practice (Girhammar and Pajari 2008; Han et al. 2010; Hassan and Rizkalla 2002; Hsu 1989; Kim et al. 2012; Lee et al. 2016; Park et al. 2019; Ren et al. 2015). Thus, an innovative construction method is required for further reducing the construction cost of PC structural systems.

For a typical duration-shortening-type PC system, which is commonly used in factories or logistics centers (Fig. 1a and b), PC beams are constructed first. Then, on top of these, PC slabs are placed (Fig. 1b). Finally, by placing reinforcement and cast-in-place (CIP) concrete, the structural integrity among the PC beam, PC slab, and PC column is secured (Fig. 1c).

*Correspondence: kangsm@ssu.ac.kr
[2] School of Architecture, Soongsil University, 369 Sangdo-ro, Dongjak-Gu, Seoul 06978, Republic of Korea
Full list of author information is available at the end of the article
Journal information: ISSN 1976-0485 / eISSN 2234-1315

(a) PC in semiconductor factory **(b)** PC in logistics factory **(c)** Typical PC

Fig. 1 Construction of typical PC beam–concrete column connection.

Recently, as a new PC construction method for improving economy and constructability, a PC double-beam system has been developed. For factories or logistics centers, a PC beam is typically divided into two beams that are parallel to each other (Fig. 2a), because a single PC beam is generally too heavy to be carried due to its large self-weight of the members. In the PC double beam–column connection, by increasing the spacing of the two parallel double beams, the span length of the PC slab can be decreased (Fig. 2b).

In the PC double beam–column connection, a PC column module, including a PC column for the current floor, a wide bracket, and a spliced PC column for the upper floor, is used (Figs. 3a and 4a). The wide bracket of the PC column module is designed to support the widely spaced PC beams, whereas the spliced PC column on the bracket enables the upper column for the next floor to be continuously constructed without placement and/or curing of CIP concrete for topping and the beam–column joint. After placing post-installed anchors on the footing (Fig. 3b), they are connected with the PC column module (Fig. 3c). On the bracket, two paralleled double beams are placed (Fig. 3d). PC or RC slabs are constructed between the PC double beams (Fig. 3e), while another PC column module is prepared and repeated for the upper floor, by using the spliced PC column with splicing sleeves (Fig. 3f and g). Finally, CIP concrete is cast for the topping and beam–column joint at each floor (Fig. 3h).

The proposed PC double beam–column connection has the following economic and structural advantages:

1) For conventional PC systems using the beam–column ramen structure, the net span length required for the design of PC slabs is typically greater than 10 m, which requires a relatively large cross section to sustain greater member force and displacement (Fig. 2a). In contrast, in the proposed double-beam PC system, by widening the spacings of the two paralleled beams, the net span length of the PC slab can be decreased to approximately 9 m, which amounts to a 10% reduction in materials (Fig. 2b).
2) Because of the shorter span length, the member forces are decreased; in particular, the flexural moment is decreased by approximately 20%, which

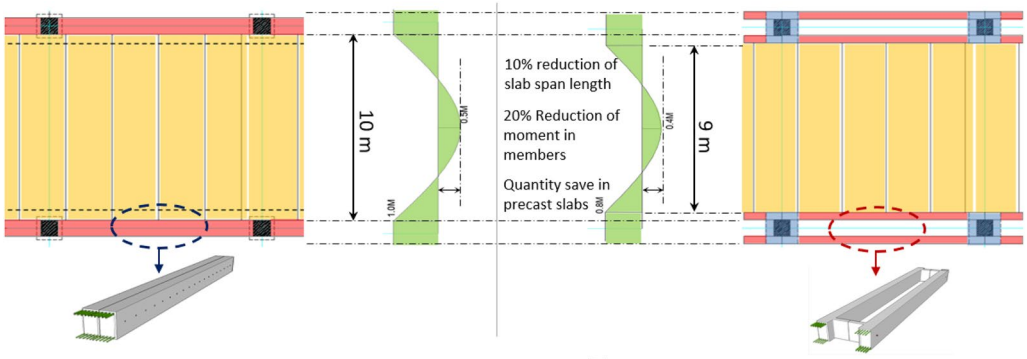

(a) Existing precast construction system **(b)** Double beam precast construction system

Fig. 2 Comparison of existing PC system and double-beam PC system.

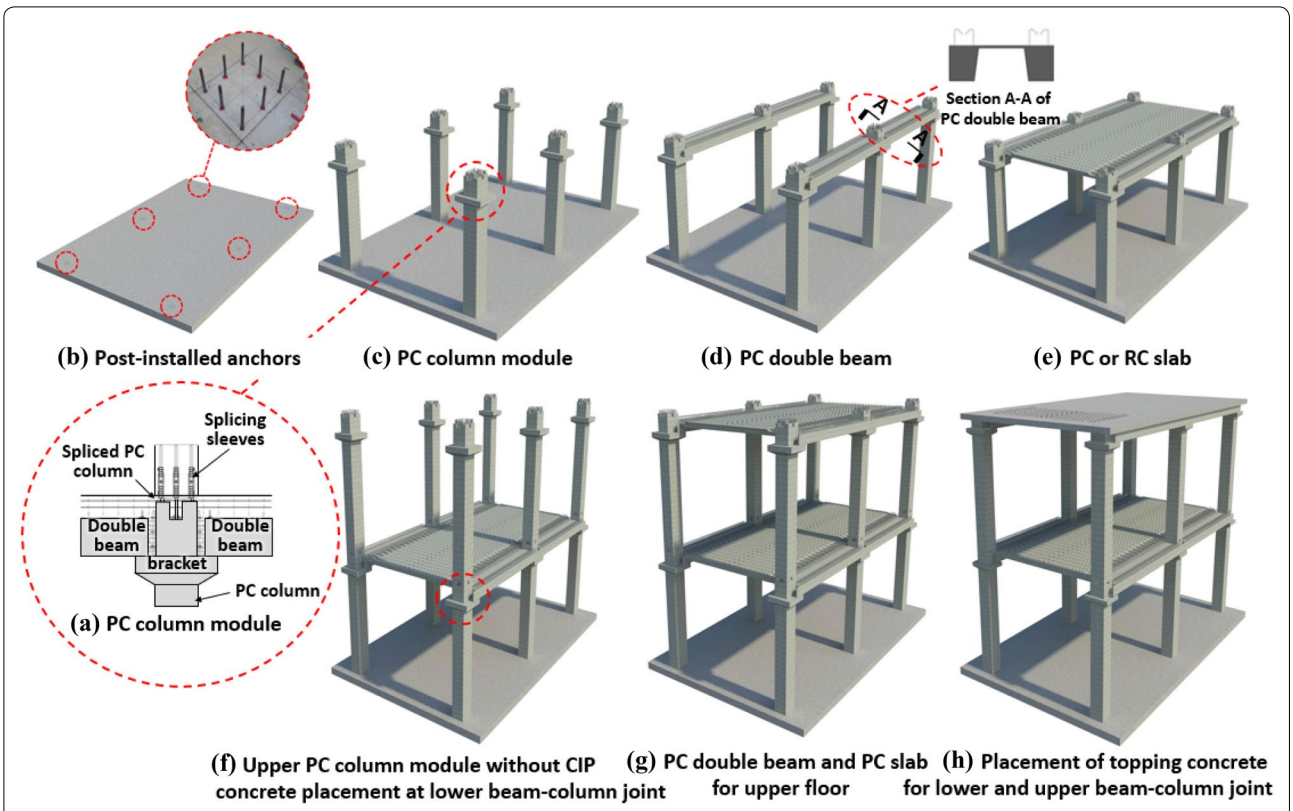

Fig. 3 Construction of PC double beam–PC column connection.

can directly decrease the required thickness of the PC slabs (Fig. 2b).

3) The upper column for the next floor can be continuously constructed prior to the placement and/or curing of CIP concrete for the topping and beam–column joint, by simply connecting to the lower PC column using splice sleeves in the spliced PC column (Fig. 3f). Thus, the construction speed of the building can be enhanced, unaffected by the CIP concrete placement of the topping, beam–column joint, and/or slab.

However, in the PC double-beam system, the bracket of the PC column and the ends of the two parallel PC beams should be eventually integrated by the CIP beam–column joint. Thus, the integrity at the PC beam–PC column connection may affect the safety of the overall system. Therefore, the integrity and structural capacity for the proposed PC double beam–column connection need to be verified.

In the present study, three specimens of PC double beams under gravity loading and three specimens of beam–column connection under cyclic lateral loading were tested, to investigate the integrity and seismic performance of the PC double beam–column connection. The test parameters included the presence of the spliced PC column and the use of an additional reinforcement at the beam–column joint. An RC specimen was also tested under cyclic lateral loading for direct comparison with PC specimens. From the results of the gravity loading test, the failure mode, flexural capacity, and integrity of the PC double-beam connection were evaluated. From the results of cyclic lateral loading test, the failure mode, strength, deformation capacity, and energy dissipation capacity of the PC double-beam specimens were compared with those of the RC double-beam specimen. Further, the seismic performances of the PC double-beam specimens were evaluated based on the acceptance criteria of moment frame in the ACI 374.1-05 (ACI Committee 374 2005) provision.

2 Design of PC Double Beam–Column Connection

2.1 Design of PC Double Beam

Figure 4a shows a PC double beam–column joint under concentrated load at both ends. To simplify the test setup, concentrated loading was used for the gravity load. Under gravity loading, the largest flexural moment typically occurs at the beam–column joint (Fig. 4a). At the beam critical section of the joint, a constant shear force was applied due to the concentrated loading

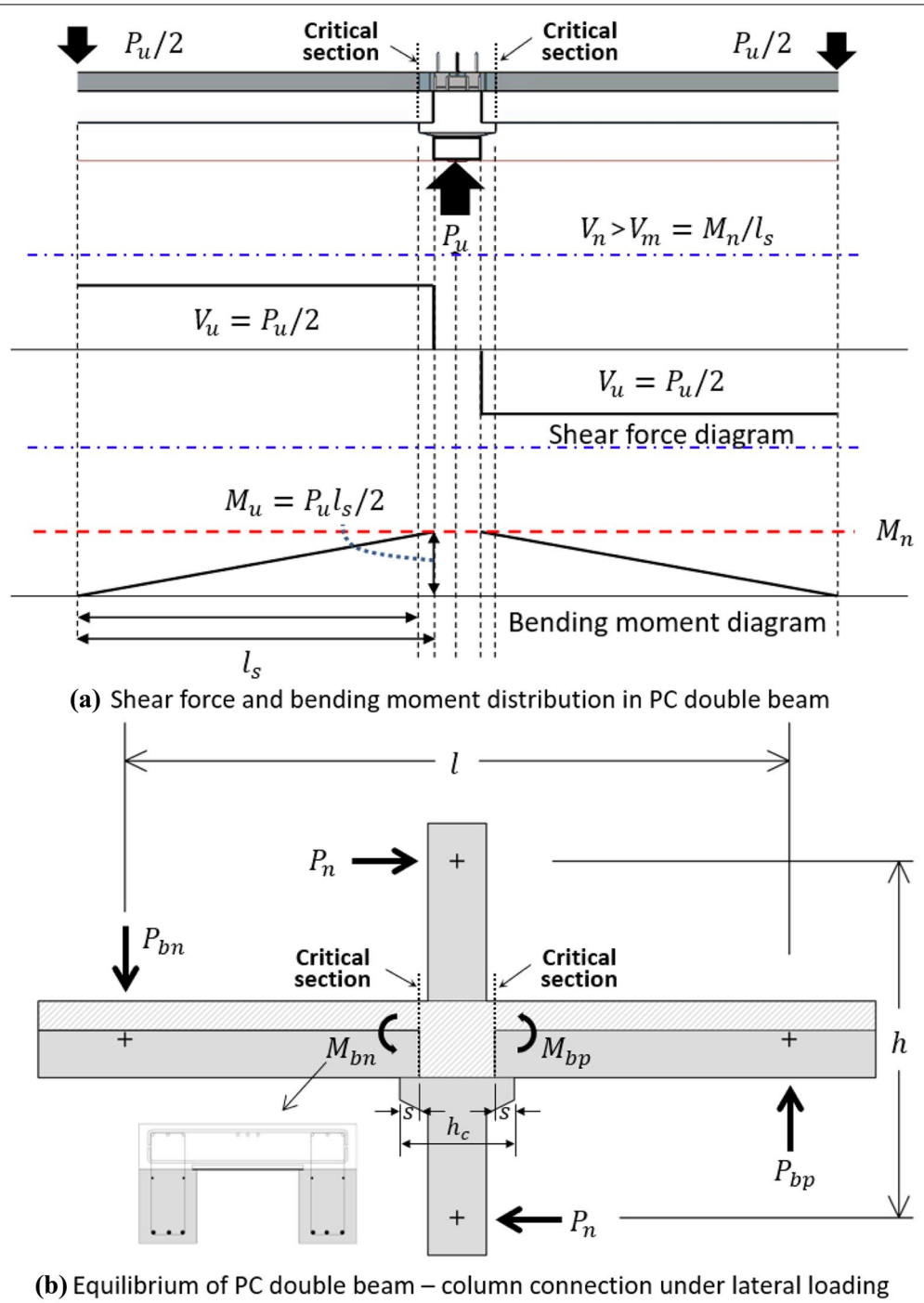

Fig. 4 Design of PC double beam–column connection.

(Fig. 4a). To avoid the brittle failure mode and to induce the ductile behavior of the beam, the specimens were designed to fail in flexure prior to shear failure at the beam–column joints. In other words, the nominal shear strength V_n of the PC beam was greater than the shear force V_m at the beam critical section, which causes flexural failure of the beam, i.e., $V_n > V_m = M_n / l_s$, where l_s = shear span length of the beam (Fig. 4a). The flexural strength of the PC double beam, M_n, specified in ACI 318 (ACI Committee 318 2019) and KCI 2012 (Korea Concrete Institute 2012) can be calculated as follows:

$$M_n = A_s f_y (d - a/2), \tag{1}$$

where A_s = area of longitudinal tension reinforcement, f_y = specified yield strength for longitudinal reinforcement, d = distance from extreme compression fiber to centroid of longitudinal tension reinforcement, a = depth of equivalent rectangular stress block.

The nominal shear strength V_n of PC beams can be calculated according to ACI 318–19 (ACI Committee 318 2019) or KCI 2012 (Korea Concrete Institute 2012) as follows:

$$V_n = V_c + V_s,$$

$$V_c = \sqrt{f_c'} bd/6,$$

$$V_s = A_s f_{yt} d/s,$$

where V_c = nominal shear strength provided by the concrete, V_s = nominal shear strength provided by transverse reinforcement, f_c' = specified compressive strength of the concrete, f_{yt} = specified yield strength of transverse reinforcement, and s = spacing of transverse reinforcement. As indicated by previous tests (Hirosawa 1977; Meinheit and Jirsa 1977), shear strength was not as sensitive to joint shear reinforcement. Thus, as required in ACI 318 (ACI Committee 318 2019) and KCI 2012 (Korea Concrete Institute, 2012), a minimum shear reinforcement was used in the specimens.

On the other hand, on the top surface of the PC double beams, topping concrete was cast during the construction and a construction joint was formed between the PC concrete and CIP topping concrete. Thus, under the applied shear V_u, a horizontal shear force V_{hv} occurs at the interface, which can be calculated using the force equilibrium shown in Fig. 5.

The nominal horizontal shear strength V_{nh} at the PC and topping concrete interface, which is intentionally roughened to a full amplitude of approximately 6 mm in general practice, can be calculated according to ACI 318–19 (ACI Committee 318 2019) or KCI 2012 (Korea Concrete Institute, 2012), as follows:

$$V_{nh} = \left(1.8 + 0.6\frac{A_v f_{yv}}{b_v s}\right) b_v d \le 3.5 b_v d, \tag{5}$$

where A_v = area of shear reinforcement within spacing s, f_{yv} = specified yield strength of shear reinforcement, b_v = width of cross section at constant surface being investigated for horizontal shear (mm), and d = distance from extreme compression fiber to centroid of longitudinal tension reinforcement. To prevent the horizontal shear failure in all specimens, the horizontal shear capacity V_{nh} was designed to be greater than the horizontal shear force V_{hv}.

2.2 Design of PC Double Beam–Column Connection

In case of an earthquake, an additional shear design of the beam–column connection should be considered (Fig. 4b). In accordance with the seismic provision of ACI 318 (ACI Committee 318 2019) and ACI-ASCE 352 (Joint ACI-ASCE Committee 352 2002), the nominal shear strength of the beam–column connections can be defined as follows:

$$V_{jn} = \gamma \sqrt{f_c'} A_j \le 1.7 \sqrt{f_c'} A_j, \tag{6}$$

where f_c' = specified compressive strength of concrete, $A_j = b_j(h_c\_2\ s)$ = effective joint shear area reduced by the seating length s of the PC beam, $b_j = \min\{0.5(b_b + b_c), b_b + h_c, b_c\}$ or $\min\{b_b + 2x, b_b + h_c, b_c\}$, where b_b = width of the beam cross section, b_c = width of the column cross section, h_c = column depth, and x = smaller perpendicular distance from the longitudinal axis of the beam to the column side. Term γ is a coefficient addressing the confinement effect of the beams framed into the joint (ACI 318 (ACI Committee 318 2019) and ACI-ASCE 352 (Joint ACI-ASCE Committee 352 2002)), and $\gamma = 1.2$ is used for the cruciform beam–column connections.

Based on the strong-column-and-weak-beam concept, assuming flexural yielding at the critical section of the beam (Fig. 4b), the joint shear demand V_{ju} at the end

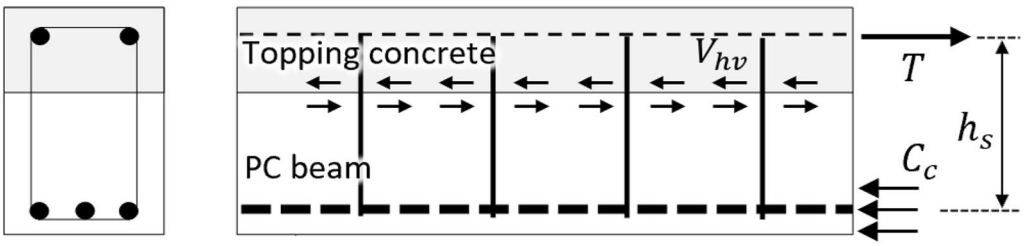

Fig. 5 Horizontal shear of PC beam.

of the PC beam–column connection can be calculated using the flexural moment demands, M_{uj} $(=M_n)$ and $M_{uj}^{'}$ $(=M_n^{'})$, which are developed by the beam moment capacity at the critical sections (Eq. 1). The joint shear demand V_{ju} is calculated as follows (ACI Committee 374, 2005; Eom et al. 2015):

$$V_{ju} = \alpha\left(C + T^{'}\right) - V_{col} \simeq \alpha\left(M_{uj} + M_{uj}^{'}\right)\frac{1}{h_s} - V_{col}, \quad (7)$$

where C and T' = resultant compression and tension forces of the beam cross sections, respectively, at the end of the PC beam; α = coefficient addressing the effects of material overstrength and cyclic strain-hardening [= 1.25; ACI 318 (ACI Committee 318 2019); ACI-ASCE 352 (Joint ACI-ASCE Committee 352 2002)]; V_{col} = shear force of the column; and h_s = distance between the top and bottom flexural bars in the beam cross section (Fig. 5).

2.3 Major Test Parameters

In the specimen names, the first letters **G** and **S** indicate specimens designed for gravity loading and seismic loading (i.e., cyclic lateral loading), respectively. Two PC double-beam systems were used for the specimens: PC system I, which had a spliced PC column at the joint prior to the placement of CIP concrete (Fig. 6a), to further reduce construction duration (**PC1** series specimens), and PC system II (Fig. 6b), where the joint was cast with CIP concrete without the spliced PC column (**PC2** series specimens), intended to increase structural integrity. **PC1** and **PC2**, following the first letter, indicate PC system I and PC system II, respectively, i.e., the presence and absence of the spliced PC column at the joint. In PC system I with a PC column at the joint, constructability can be further increased and construction duration can be reduced by continuously constructing the upper PC columns connected to the spliced column prior to the CIP concrete placement at the joint. On the other hand, in the presence of the spliced PC column at the panel zone of the beam–column joint, the connection integrity may be degraded. Thus, PC system II, without the spliced PC column at the joint, was also investigated. The **AF** following—(dash) indicates the use of additional flexural rebars at the beam–column joint. Local failure may degrade the integrity in the proposed beam–column connection. The use of additional reinforcement at the joint was considered to relocate the plastic hinge to the beam's inner section and to prevent local failure.

3 Gravity Loading Test for PC Double Beam

In the gravity loading test, the flexural behavior of the PC double beam with **PC1** and **PC2** types (Fig. 6a and b, respectively) was investigated, focusing on the composite action at the PC-beam critical section. In the calculation of Eq. (1) for the PC double beam, it was assumed for (1) a fully composite action between the PC beams and topping concrete of the beam cross section and (2) the yielding of the longitudinal reinforcement. These assumptions were validated under gravity loading by investigating the actual tested strength and strain of the longitudinal rebar. The effect of additional reinforcement at the beam–column joint to relocate a plastic hinge to the inner beam section was also investigated.

3.1 Test Specimens

Table 1 shows the major parameters of the specimens. Three specimens were prepared for half-scaled PC double beam under gravity loading. Figure 7 shows the details of the joint, dimensions, and reinforcement of the specimens. The dimensions of the column section were 420 mm × 420 mm (Fig. 7a). The shaded and void

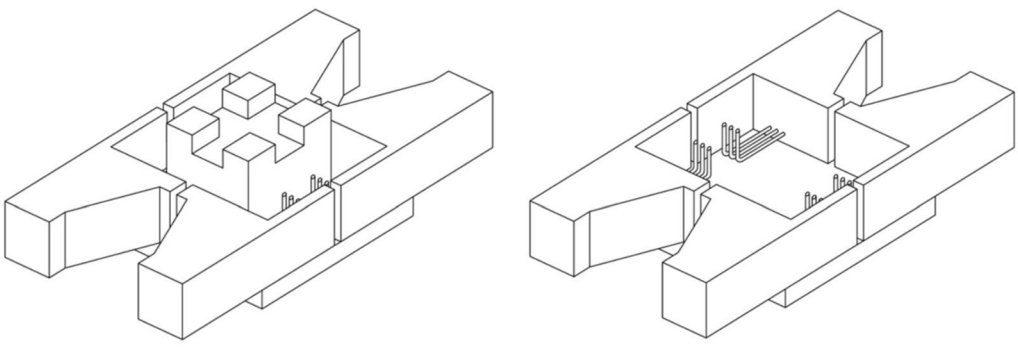

(a) PC system I (GPC1, GPC1-AF, and SPC1) (b) PC system II (GPC2-AF and SPC2)

Fig. 6 Two PC double systems used in specimens.

Table 1 Properties of test specimens.

Specimen	Concrete compressive strength (MPa)				Beam				Shear strength (kN)		
	Lower column (bracket)	Double beam	Upper column	CIP concrete	Top|bottom rebars	$d_P \| d_N$ [a] (mm)	M_n [b] (kN·m) [Eq. 1]	P_n [c] (kN)	Vertical V_n [Eq. 2]	Horizontal V_{nh} [Eq. 5]	Joint shear strength V_{jn} [Eq. 6]
GPC1	34.8	34.8	34.8	27.7	14D13|4D19	500	433	414	1206	4431	–
GPC1-AF	34.8	34.8	34.8	27.7	14D13|4D19	500	492	471	1206	4431	–
GPC2-AF	34.8	34.8	None	27.7	14D13|4D19	500	492	471	1206	4431	–
SRC	40.3		40.5	none	9D13|6D16	500|500	301|292	239	1340	3195	1238
SPC1	38.4	41.8	41.8	40.3	9D13|4D16	500|500	210|292	188	1340	3195	1261
SPC2	41.8	41.8	none	40.3	9D13|4D16	500|500	210|292	188	1340	3195	1261

[a] d_P and d_N = effective depths of beam cross sections for positive and negative moments [Fig. 7b and c].

[b] Positive moment | negative moment.

[c] P_n was calculated using $2M_n/l_s$ (Fig. 4a) for specimens **GPC1**, **GPC1-AF**, and **GPC2-AF** under gravity loading, whereas for specimens **SRC**, **SPC1**, and **SPC2** under cyclic lateral loading, P_n was calculated using Eq. (8).

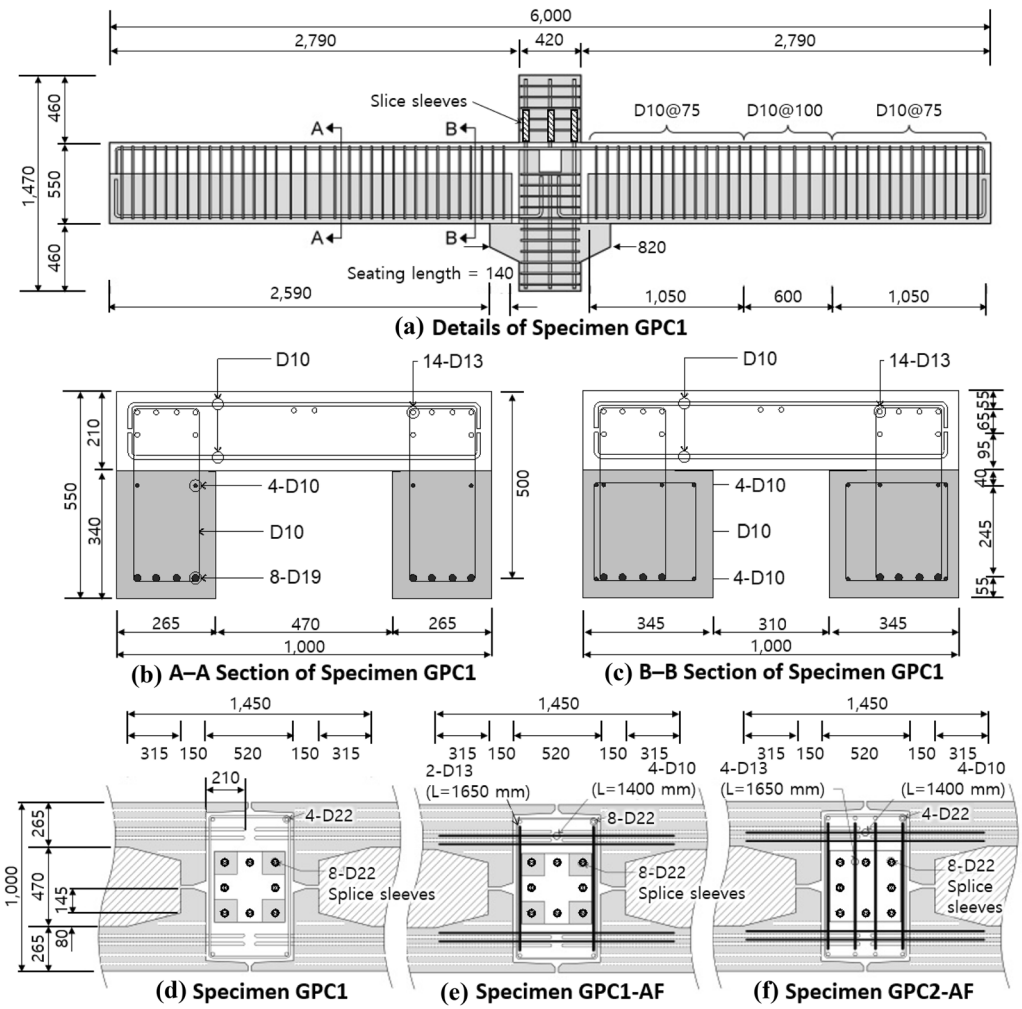

Fig. 7 Configuration and reinforcement details of test specimen under gravity loading.

areas in Fig. 7 indicate the PC concrete and CIP concrete, respectively.

In **GPC1**, PC double beams and a spliced PC column at the joint were integrated by CIP concrete placement of the topping and beam–column joint (Figs. 6a and 7a). 14-D13 bars and 8-D19 bars were used for the upper and lower (i.e., tension and compression) longitudinal reinforcement in CIP topping concrete and PC double beams, respectively (Fig. 7 b and c); thus, the nominal flexural moment of the beam section, M_n, was calculated as 432.8 kN·m using Eq. (1). On the other hand, in the PC beam–column joint, it is difficult to satisfy the required development length of the lower (compression) longitudinal rebars in seismic provisions of the design codes (ACI Committee 318 2014; ACI Committee 374 2005; Korea Concrete Institute 2012), because of the rebar interference at the joint (Fig. 7d). Thus, for specimens under gravity loading, the development length l_d of the lower flexural rebars was 210 mm, which was shorter than the design development length of Type 2 beam–column connection (Joint ACI-ASCE Committee 352 2002): $\alpha f_y d_b/(6.2\sqrt{f_c'}) = 370$ mm, where α is a stress amplifier (= 1.25). For transverse reinforcement of the beams, D10 bars were used. The spacing was 75 mm near the joint and 100 mm at the beam center (Fig. 7 a). Thus, the nominal shear strength of the beam section, V_n, was calculated as 1,206 kN using Eqs. (2) to (4). On the other hand, the nominal horizontal shear strength at the PC concrete–CIP concrete interface of the beam section, V_{nh}, was calculated as 4,431 kN using Eq. (5), which was significantly higher than the expected horizontal shear demand ($\approx A_s f_y = 908$ kN).

In **GPC1-AF**, a plastic hinge relocation method (Dalalbashi et al. 2012; Eom et al. 2015; Joh et al. 1991; Juette 1996; Yamamoto et al. 2008) was used to prevent a local failure, which is expected to degrade the integrity

near the beam–column joint. In addition, 4-D10 flexural rebars and 2-D13 stirrups enclosing the flexural reinforcement were placed (Fig. 7e). Thus, the nominal flexural moment of the beam critical section, M_n, was increased to 492.3 kN·m through the additional flexural rebars. However, considering the constructability of the PC system, the lengths of the additional flexural rebars and stirrups were limited to 1400 and 1650 mm, respectively (Fig. 7e). The other details of **GPC1-AF** are identical to those of **GPC1**.

In **GPC2-AF**, to investigate the effect of the non-spliced PC column at the joint on joint integrity, no spliced PC column was used at the joint. Instead, the CIP topping concrete was directly filled in the beam–column joint (Figs. 6b and 7f). The reinforcement details of **GPC2-AF** are identical to those of **GPC1-AF**, except for two additional stirrups (4-D13) enclosing the flexural reinforcement (Fig. 7f).

The material tests were performed on the day of testing. Three concrete cylinders each were tested for the PC members cast with the same concrete, including the bracket, PC beam, and spliced PC column at the joint (if present), and for the CIP concrete at the topping and beam–column joint. Table 1 presents the average values of the compressive strength. The concrete compressive strength was 34.8 and 27.7 MPa for the PC members and CIP concrete, respectively. Three coupons each were tested for the rebar used in the specimens. The average values of yield strength and tensile strength are presented in Table 2. For D10, D13, and D19 bars used for the specimens under gravity loading, the yield strength was 551.9, 512, and 509.7 MPa, respectively (Table 2).

3.2 Construction Sequence

Figure 8 shows the construction of the PC double-beam system. Each PC member was fabricated prior to the assembly (Fig. 8a). In case of **GPC1** and **GPC1-AF**, on top of the bracket, PC double beams and a spliced PC column were located and the CIP concrete covering the upper part of the PC double beams and the beam–column joint was cast (Fig. 8b). Owing to the pre-occupied spliced PC column, the upper PC column could splice to the longitudinal rebars of the lower column using the splice sleeves prior to the placement of the CIP concrete (Fig. 7a). In case of **GPC2-AF** without splicing, the PC column at the joint, only PC double beams were located and CIP concrete was filled in the upper part of the PC double beams and the beam–column joint, including the void, due to the absence of the PC column (Fig. 8c). Because of the absence of the spliced PC column at the joint, the upper PC column was spliced after the placement of the CIP concrete.

3.3 Test Methods

A monotonic loading was applied to the specimens (Fig. 9a), which were turned upside down for convenience of loading. Simply supported by the beam ends, the beam was subjected to a concentrated loading at the bottom of the bracket. Figure 9a shows the location of the linear variable differential transducers (LVDTs) for measuring each displacement of the specimens.

3.4 Failure Mode

Figure 10 shows the crack pattern and failure mode of the specimens under gravity loading at the end of the test. Regardless of the parameters, the crack patterns and failure modes were similar to each other. Typical flexural cracks were dominant at the tension zone throughout the tests. At the end of the test, the concrete crushing at the compression zone occurred near the section of the beam–bracket contact surface (Fig. 10), which indicates that the critical section was the interface of the PC beam and PC bracket. Other failures, such as local bearing failure, anchorage failure, and/or horizontal shear failure, did not occur.

3.5 Load–Displacement Relations

Figure 11 shows the load–displacement relation of the specimens under gravity loading. The vertical load was measured at the actuator mounted on the bracket, while the displacement was measured at the upper column of the specimen by LVDTs 1 and 2 located at the center (Fig. 9a). The figures also shows the nominal flexural strength P_n based on the actual material strength in

Table 2 Properties of reinforcement.

Bar type		D10	D13	D16	D19	D22	D22
Bar grade, MPa		400					600
Bar diameter, mm		9.53	12.7	15.9	19.1	22.2	22.2
Yield strength f_y, Pa	Gravity loading test (**GPC1**, **GPC1-AF**, and **GPC2-AF**)	551.9	512.0	–	509.7	–	–
	Cyclic loading test (**SRC**, **SPC1**, and **SPC2**)	557.8	527.9	500.9	510.4	544.8	662.7
Tensile strength f_u, MPa	Gravity loading test (**GPC1**, **GPC1-AF**, and **GPC2-AF**)	650.8	634.5	–	615.9	–	–
	Cyclic loading test (**SRC**, **SPC1**, and **SPC2**)	680.3	650.0	642.7	656.5	667.8	764.4

(a) Placement of reinforcement and concrete in PC double beams

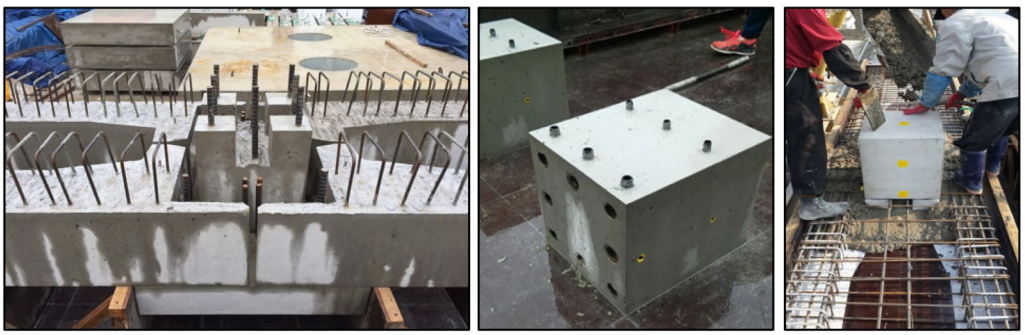

(b) PC double beams + PC column + CIP RC topping (**Specimens GPC1 and GPC1-AF**)

(c) PC double beams + CIP RC topping (**Specimen GPC2-AF**)

Fig. 8 Construction of test specimen under gravity loading.

Tables 1 and 2, which was calculated as two times the nominal sectional flexural moment at the beam near the joint divided by the span length l_s: $P_n = 2M_n/l_s$ (Fig. 6a). Note that the nominal flexural moment, M_n, was calculated by ACI 318 (ACI Committee 318 2019) under the assumptions of (1) the composite action of the PC double-beam sections (the PC double beams and topping concrete and (2) the yielding of the tension longitudinal reinforcement.

In **GPC1**, with the PC double beams, spliced PC column, and CIP concrete (Fig. 11a), the peak strength P_{test} was 501 kN, which was 21% greater than the predicted flexural strength P_n (=414 kN). This indicated that the composite action assumed for the PC double beam is valid, and that the moment capacity can be predicted by the current design prediction. At the yielding displacement δ_y of 15 mm, the load-carrying capacity P_y was 375 kN. With an increase in the vertical displacement, the load-carrying capacity was further increased after yielding, which is attributable to strain-hardening of the rebars. The load-carrying capacity was decreased to 75% of the peak strength at an ultimate displacement of $\delta_u = 170$ mm. Thus, the ductility ratio μ was 11.3 ($=\delta_u/\delta_y$). The definitions of yield displacement δ_y, ultimate displacement δ_u, and ductility ratio μ are presented in Fig. 11d.

In **GPC1-AF** (Fig. 11b) with additional reinforcement at the beam–column joint (Fig. 7e), the peak strength

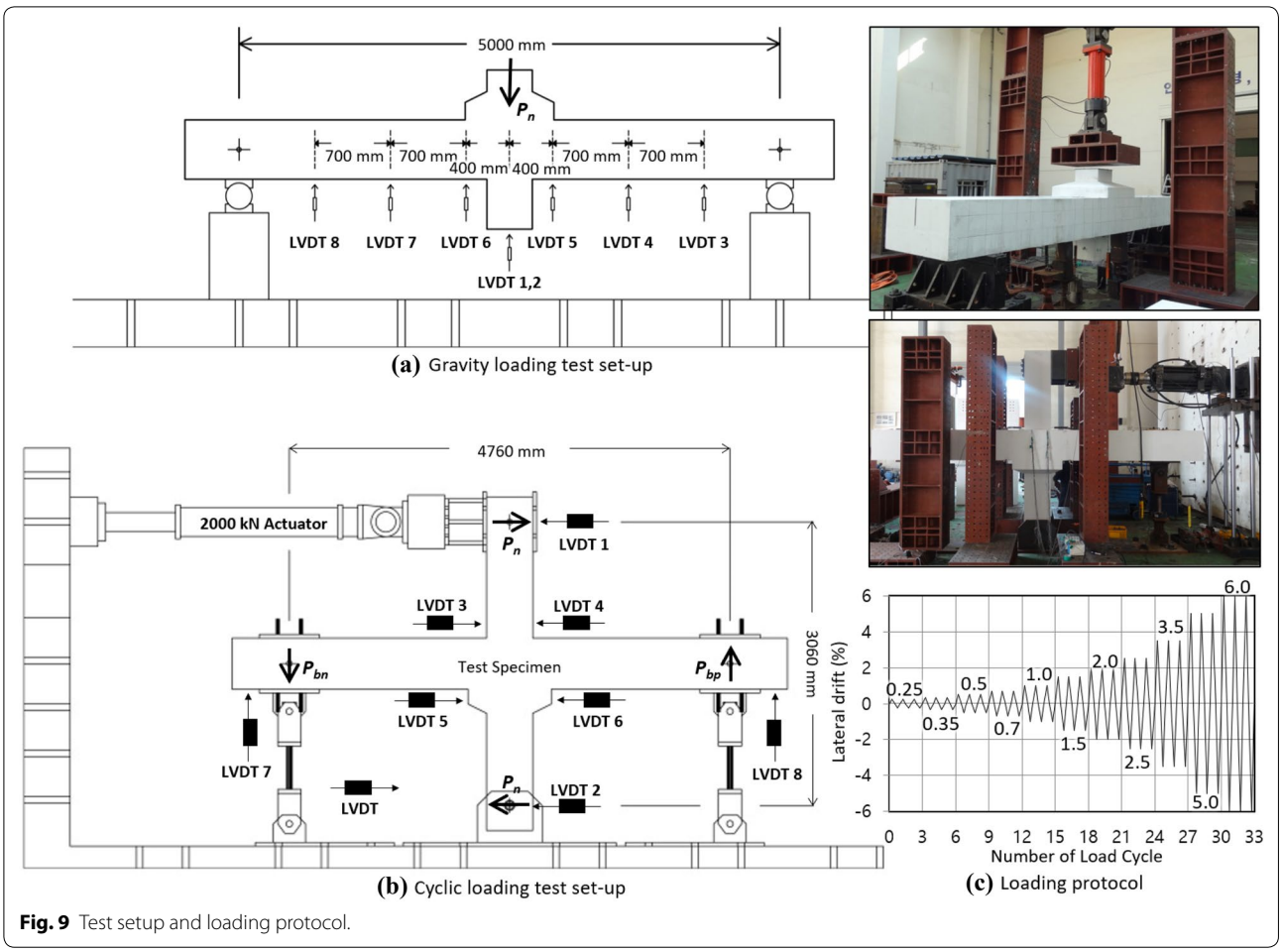

Fig. 9 Test setup and loading protocol.

was increased to 523 kN, which was 11% greater than the predicted flexural strength P_n (=471 kN). The peak strength was only 4% greater and the strength ratio was 10% smaller than that of **GPC1** without additional reinforcement at the beam–column joint. Further, unlike **GPC1**, as the displacement increased after yielding, the load-carrying capacity was not increased. This is because the development length of the additional flexural rebars is insufficient, and therefore, they are limited to experience strain-hardening, which increases the flexural strength. The ductility ratio was $\mu = 11.7$ ($= [\delta_u/\delta_y] = [158.7\text{ mm}/13.6\text{ mm}]$), which was comparable to that of **GPC1**.

In **GPC2-AF** (Fig. 11c), without the PC double column at the joint and with the additional reinforcement at the beam–column joint (Fig. 7f), the load-carrying capacity was similar to that of **GPC1-AF** with the PC column at the joint. This result indicates that the PC column at the beam–column joint does not significantly affect the structural performance under gravity loading.

3.6 Strain of Reinforcing Bars

Figure 12a shows the locations of strain gauges for measuring the strains of the tension longitudinal rebars. For **GPC1-AF** and **GPC2-AF**, locations of strain gauges for the additional flexural rebars are also presented.

Figure 12b shows the rebar strain–central displacement relations for **GPC1**, with the PC double beams, spliced PC column, and CIP topping concrete. The strains of the longitudinal rebars were the largest at the bracket–beam interfaces (FC, FE), reaching the yield strain at approximately 15 mm, which coincided with the yield displacement δ_y estimated through the definition in Fig. 11d. As the measured location was farther away from the beam–column interface, the strain was decreased (FB, FF). At the locations of FB and FF, 500 mm away from the critical section, yielding of the flexural rebars occurred. In contrast, at the location of FA and FG, 1000 mm away from the critical section, yielding of the flexural rebars did not occur throughout the test. This result indicates that the plastic hinge length l_p of the PC double beam was greater than the effective depth of the beam, d (=500 mm) (Bae

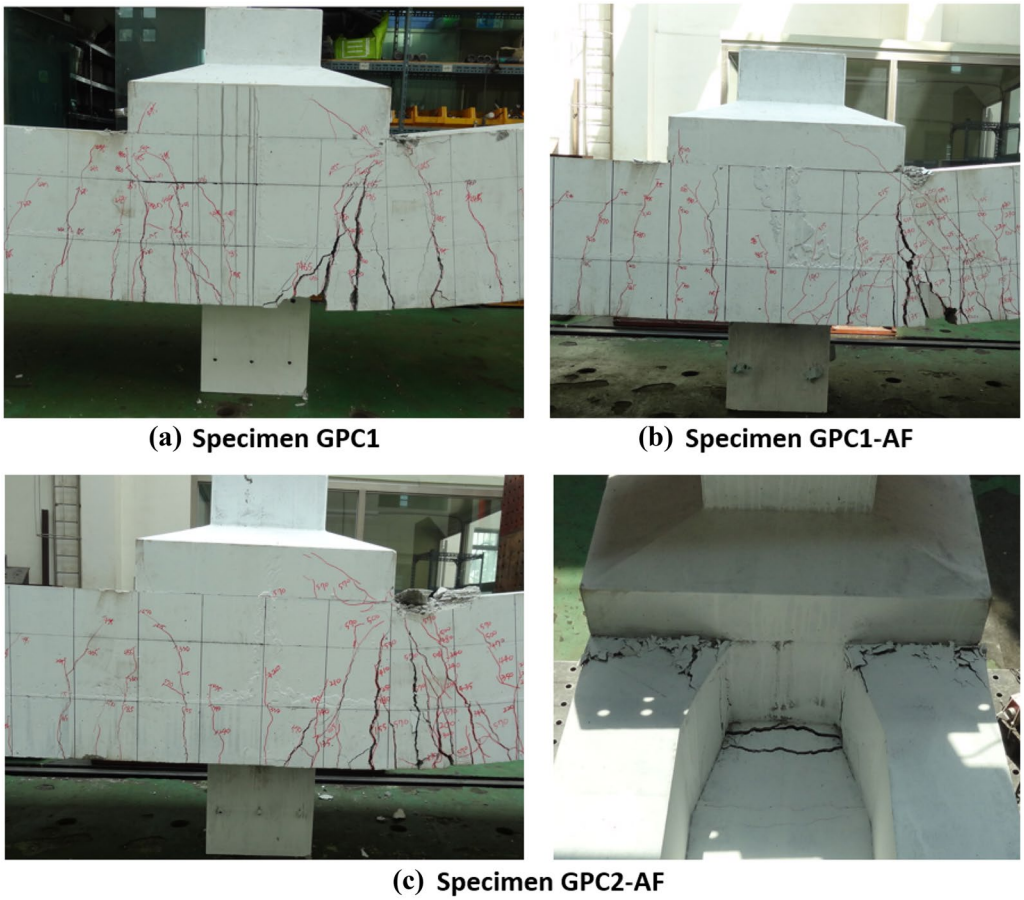

Fig. 10 Damage modes of specimens under gravity loading at the end of the test.

and Bayrak 2008; Corley 1966; Panagiotakos and Fardis 2001; Paulay and Priestley 1992). The rebar strains in **GPC1-AF** and **GPC2-AF** were close to those in **GPC1**.

In **GPC1-AF** and **GPC2-AF** with additional flexural rebars (Fig. 12c), similar to the other flexural rebars, as the measured location was farther away from the critical section, the strain was decreased (AFB). Although the yielding of the flexural rebars occurred at the center of the rebar (AFD), the flexural rebar strain continuously decreased with a further increase in displacement (approximately after 70 mm). This result indicates that the effect of additional flexural rebars within the inelastic range was limited due to the lack of the bar development length engaged in the plastic hinge location.

In summary, regardless of the presence of the spliced PC column at the beam–column joint, the current design flexural strength, M_n (Eq. 1), was achieved, showing the composite action assumed for the PC double beam. On the other hand, the effect of additional reinforcement was negligible due to insufficient anchorage length. To reinforce the PC double beam–column joint, it is necessary to secure a sufficient anchorage length of the additional reinforcement outside the plastic hinge length.

4 Cyclic Loading Test for PC Double Beam

In the cyclic lateral loading test, the seismic capacities of two types of PC beam–column connections (PC1 and PC2 series (Fig. 6)) were evaluated on the basis of the acceptance criteria of moment frame in the ACI 374.1–05 (ACI Committee 374 2005) provision, and compared with that of a conventional RC double beam–column connection.

4.1 Test Specimens

Table 1 shows the major parameters of the specimens, and Fig. 13 shows the details of the joint, dimensions, and reinforcement of the specimens. Three specimens of half-scaled PC double beam–column connection were prepared for testing under cyclic lateral loading: one specimen for the RC double beam–column connection (**SRC**) and two specimens for the PC double beam–column connection (**SPC1** and **SPC2**): for specimen

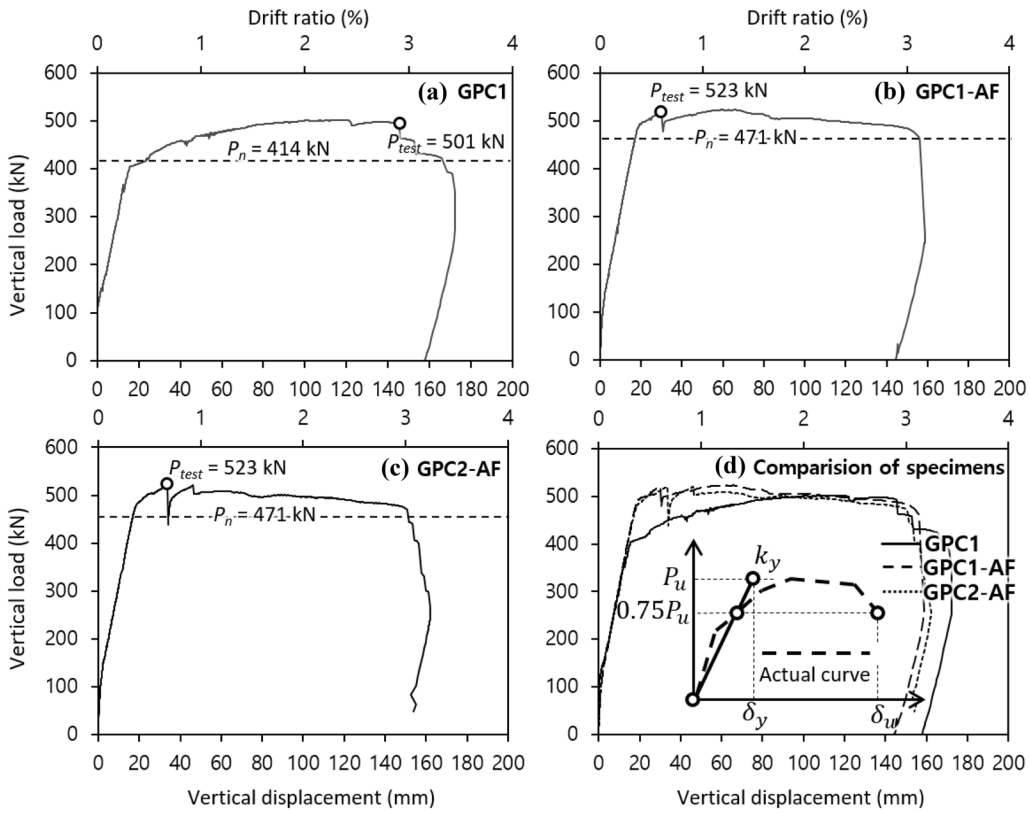

Fig. 11 Load–drift relations of specimens under gravity loading.

names, refer to **Major test parameter**. Using the strong-column-and-weak-beam concept, flexural yielding was designed at the beams in all specimens. For **SPC1**, similar to **GPC1**, **GPC1-AF**, and **GPC2-AF**, a spliced column was used to splice the upper PC column. The dimensions of the column section were increased from 420 mm × 420 mm to 500 mm × 500 mm to prevent an early failure of the PC columns (Fig. 13).

In **SRC** (Fig. 13a), conventional RC was used for the double beam–column connection. Then, 9-D13 and 6-D19 bars were used for the upper and lower longitudinal reinforcement, respectively (Fig. 13b and c); thus, the positive and negative values of M_n were calculated as 302 and 292 kN·m, respectively (Table 1). For transverse reinforcement of the beams, D10 bars were used, with spacings of 75 mm near the joint and 100 mm at the beam center (Fig. 13b and c).

In **SPC1** (Fig. 13d), similar to **GPC1** (or **GPC1-AF**) (Fig. 7a–e), PC double beams, a spliced PC column at the joint, and CIP concrete for topping at the upper part of the double beam and beam–column joint were used. As shown in Fig. 7d for test specimens under gravity loading, 4-D16 bars among 6-D16 bars for lower reinforcement were anchored into cast-in topping concrete at beam–column joint; therefore the positive and negative values of M_n were calculated as 210 and 292 kN·m, respectively (Table 1). To satisfy the required development length of the lower longitudinal rebars in seismic provisions of ACI 318 (ACI Committee 318 2019) and KCI 2012 (Korea Concrete Institute 2012), as well as to avoid the rebar interference at the joint, alternative placement was used (Fig. 13d). Thus, the development length l_d of the lower longitudinal rebars was 380 mm, which was greater than the design development length of Type 2 beam–column connection (Joint ACI-ASCE Committee 352 2002): $\alpha f_y d_b/(6.2\sqrt{f_c'}) = 255$ mm, where α is a stress amplifier (= 1.25). The other details of **SPC1** are identical to those of **SRC**. The nominal shear strength at the PC concrete–CIP concrete interface of the beam section, V_n, was calculated as 1,340 kN using Eqs. (2) to (4). On the other hand, the nominal horizontal shear strength of the beam section, V_{nh}, was calculated as 3,195 kN using Eq. (5), which was significantly greater than the expected horizontal shear demand ($= A_s f_y = 397.9$–636 kN).

In **SPC2** (Fig. 13e), similar to **GPC1-AF** (Fig. 7e), the PC double beams and CIP concrete for the topping and

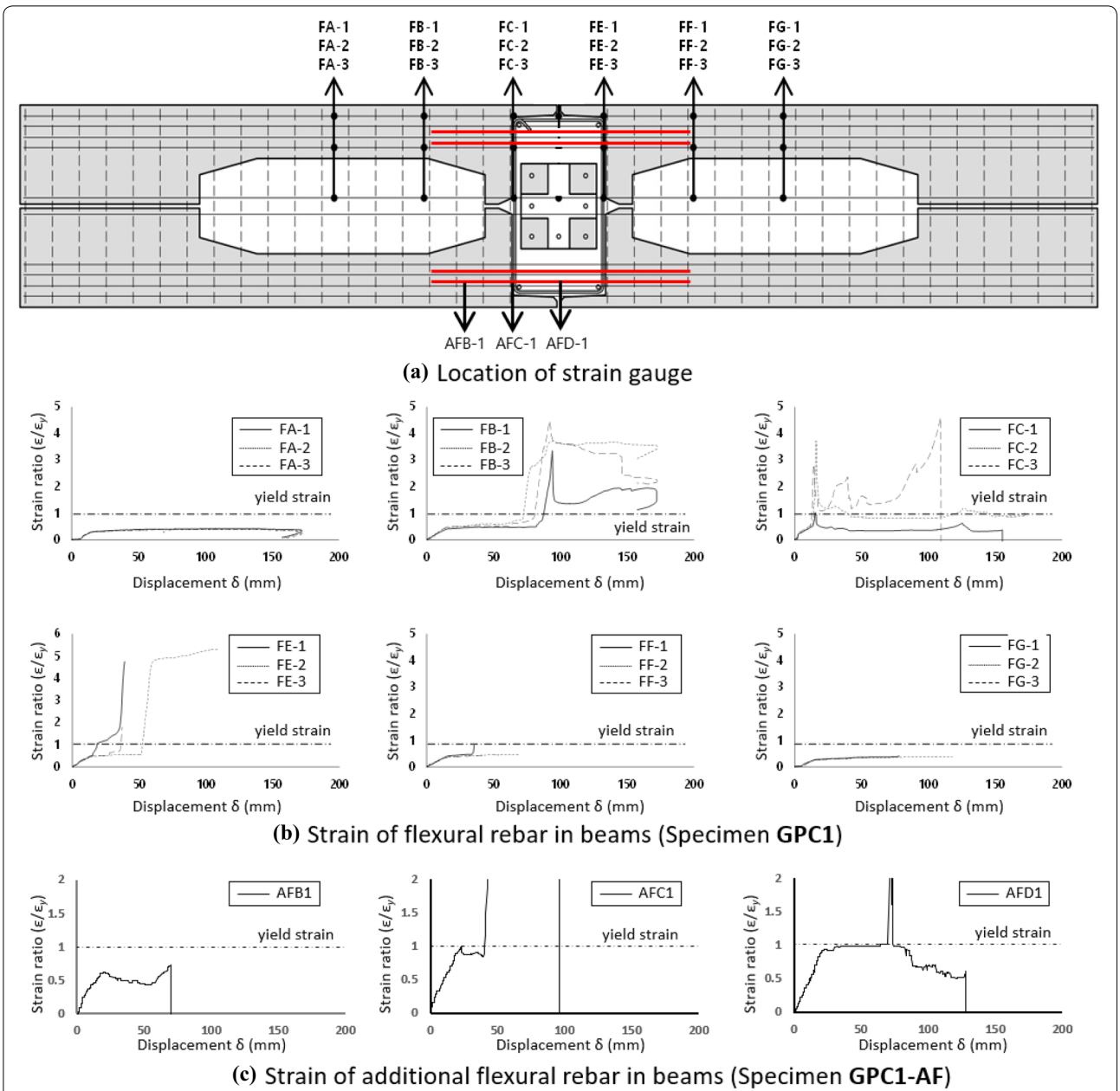

Fig. 12 Strain of flexural reinforcing bar in beams of specimens under gravity loading.

beam–column joint were used without any spliced PC column at the joint. The other details of **SPC2** are identical to those of **SPC1**.

According to the similar construction sequences of **GPC1** (or **GPC1-AF**) and **GPC2-AF**, the upper PC column was spliced to the longitudinal rebars of the lower PC column prior to and after the CIP concrete placement in **SPC1** with the spliced PC column at the joint and **SPC2** without the spliced PC column at the joint (Fig. 13d and e).

The material tests were performed on the day of testing. Three concrete cylinders each were tested for the lower column, double beams, and CIP concrete for the upper part of the PC double beam and beam–column joint. The average values of the compressive strength are presented in Table 1. In **SRC** with a conventional RC double beam–column connection, the concrete for the lower column and beam was cast simultaneously (=40.3 MPa in Table 1), followed by concrete placement for the upper column (=40.5 MPa in Table 1). The concrete

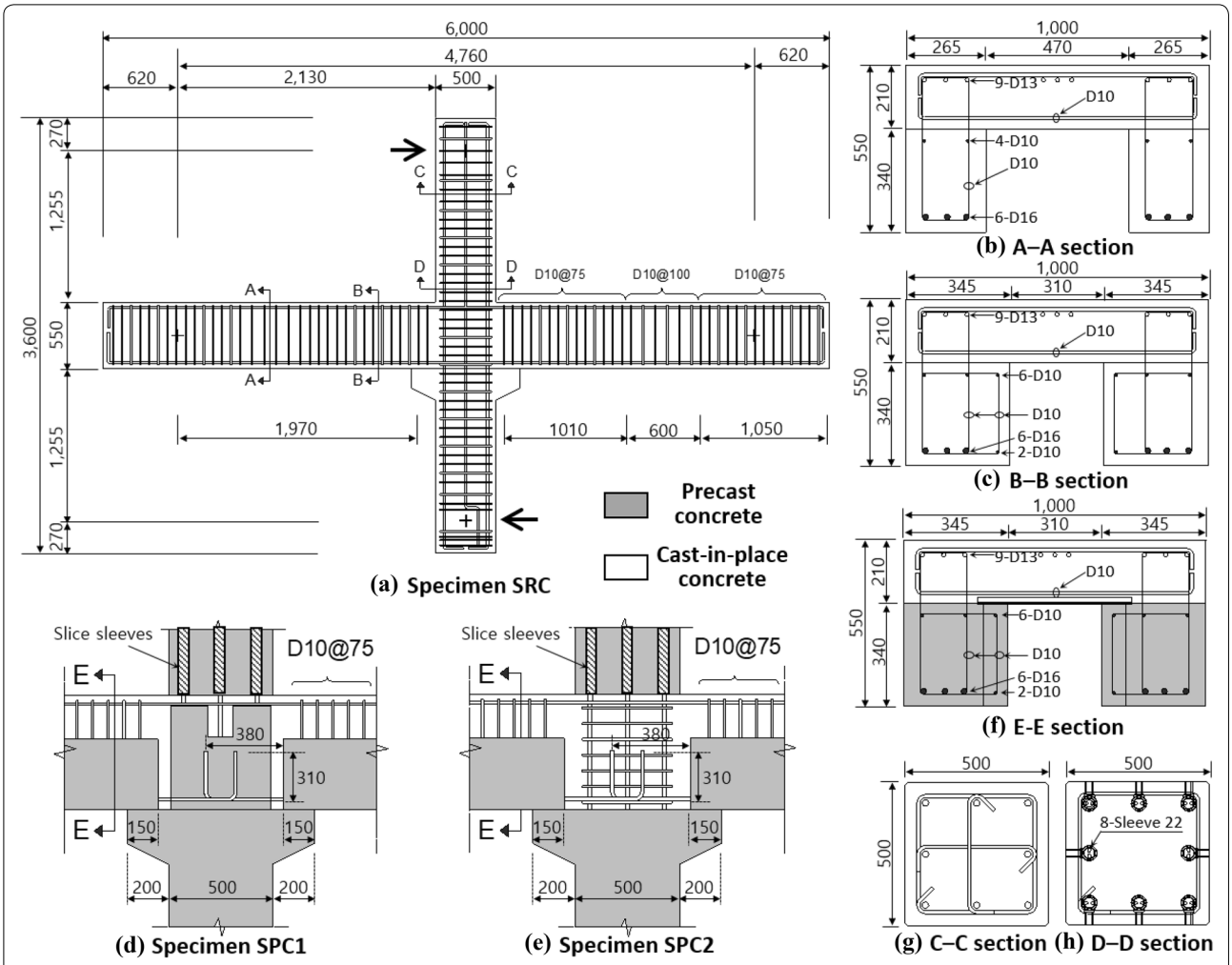

Fig. 13 Configuration and reinforcement details of test specimen under cyclic lateral loading.

compressive strength ranged from 38.4 to 41.8 MPa. Three coupons each were tested for the rebar used in the specimens. The average values of the yield strength and tensile strength are presented in Table 2. The yield strengths of D10, D13, D16, D22 (Grade 400 MPa), and D22 (Grade 600 MPa) bars were 574, 521, 521, 506, 552, and 649 MPa, respectively (Table 2).

4.2 Test Setup

A cyclic lateral loading was applied to the specimens, as shown in Fig. 9b. The lower part of the column was hinge-supported, while both beam ends were roller-supported. The upper part of the column was hinge-connected with the actuator, which moved in the horizontal direction under displacement control. Figure 9b also shows the linear variable displacement transducers (LVDTs) for measuring lateral displacements (LVDT 1), slip at the column hinge (LVDT 2), and vertical extension and contraction of the roller supports measured at the hinges at both beam ends (LVDTs 7 and 8). The loading protocol was planned as shown in Fig. 9c; at initial loading, the story drift ratio was 0.25% and the following drift ratio was 1.5 times the previous one until a maximum drift ratio of 6.0% was achieved, with three cycle repetition at each drift ratio (ACI Committee 374 2005). Axial force generally increases the shear strength of the joint (Masi et al. 2013; Paulay and Priestley 1992a, b). However, axial load was not applied to the columns in this study to simplify the tests and to create severe loading condition for the joint (Fenwick and Irvine 1977).

4.3 Failure Mode

Figure 14 shows the crack pattern and failure mode of the specimens under cyclic lateral loading at the end of the test.

Fig. 14 Damage modes of specimens under gravity loading at the end of the test.

In **SRC** with a conventional RC double beam–column connection (Fig. 13a to c), initial cracks occurred at the beam–column joint and column. As the drift ratio increased, the cracks at the joint and horizontal cracks between the upper bracket and joint were propagated (Fig. 14a).

In **SPC1** and **SPC2** with a PC double beam–column connection (Fig. 13(d) and (e)), cracks occurred at the beam–column joint and columns at the initial loading (Fig. 14b and c). As the drift ratio increased, the extensive cracks occurred at the interfaces between the PC beams and CIP concrete. The drift ratio at failure was 5.6%–5.9% in **SPC1**, which was slightly smaller than that of **SRC** with RC double beam–column connection (6.0%–6.2%). The failure mode was not affected by the presence (**SPC1**) and absence (**SPC2**) of the PC column at the joint.

4.4 Load–Displacement Relationships

Figure 15 shows the lateral load–displacement (drift ratio) relationships of the specimens under cyclic lateral loading. The lateral displacement indicates the net displacement, excluding slip at the column hinge (LVDT 2 in Fig. 9b) and extension and contraction of the roller supports (LVDTs 7 and 8 in Fig. 9b). The lateral drift ratio was divided by the net column height ($h = 3060$ mm).

Table 3 presents the maximum strength P_{test}, yield drift ratio δ_y, yield stiffness k_y, and maximum drift ratio δ_u. In Fig. 15d, k_y is defined as the pre-peak secant stiffness corresponding to $0.75P_{test}$. The yield drift ratio was calculated as $(P_{test}/k_y)/h$. The maximum drift ratio δ_u is defined as a post-peak drift ratio corresponding to $0.75P_{test}$ (Park 1988).

In **SPC1** (Fig. 15b) with a PC double beam–PC column connection, the overall behavior was similar to that of **SRC** (Fig. 15a) with the conventional RC double beam–column connection. After yielding, the load-carrying capacities of both **SRC** and **SPC1** gradually increased. The peak strength of **SPC1** with the PC double beam–column connection was + 218 kN and -254 kN in the positive and negative loading directions, respectively, which were 22% and 9% smaller than those of **SRC** with the RC double beam–PC column connection. The maximum drift ratio of **SRC** ($\delta_u = 6.0\%–6.2\%$) was slightly greater than that of **SPC1** ($\delta_u = 5.6\%–5.9\%$).

In **SPC2** (Fig. 15c) with the PC double beam–column connection but without the spliced PC column at the joint, the load-carrying capacity was similar to that of **SPC1** with the spliced PC column at the joint, which indicates that the PC column at the joint had negligible effect.

The disparity of the load-carrying capacity between **SRC** and **SPC** is discussed in *Evaluation of Structural Performance* in detail.

4.5 Rebar Strain

Figure 16 compares the normalized strains ($\varepsilon/\varepsilon_y$) of the flexural bars in **SRC** with the RC double beam–column connection and **SPC2** with the PC double beam–RC column connection, where normalized strains were obtained based on the material test results (i.e., $\varepsilon_y = f_y/E_s$). Figure 16 also shows the locations of strain gauges FC (top bar) and BFC (bottom bar) within the joint, and those of strain gauges FB (top bar) and BFB (bottom bar) outside the joint.

In the top bars of **SRC** with the RC double beam–column connection (left-hand side of Fig. 16a), the strain of FC within the joint was six times the yield strain, while that of FB outside the connection was maintained in the elastic range at the initial stage. As the drift ratio

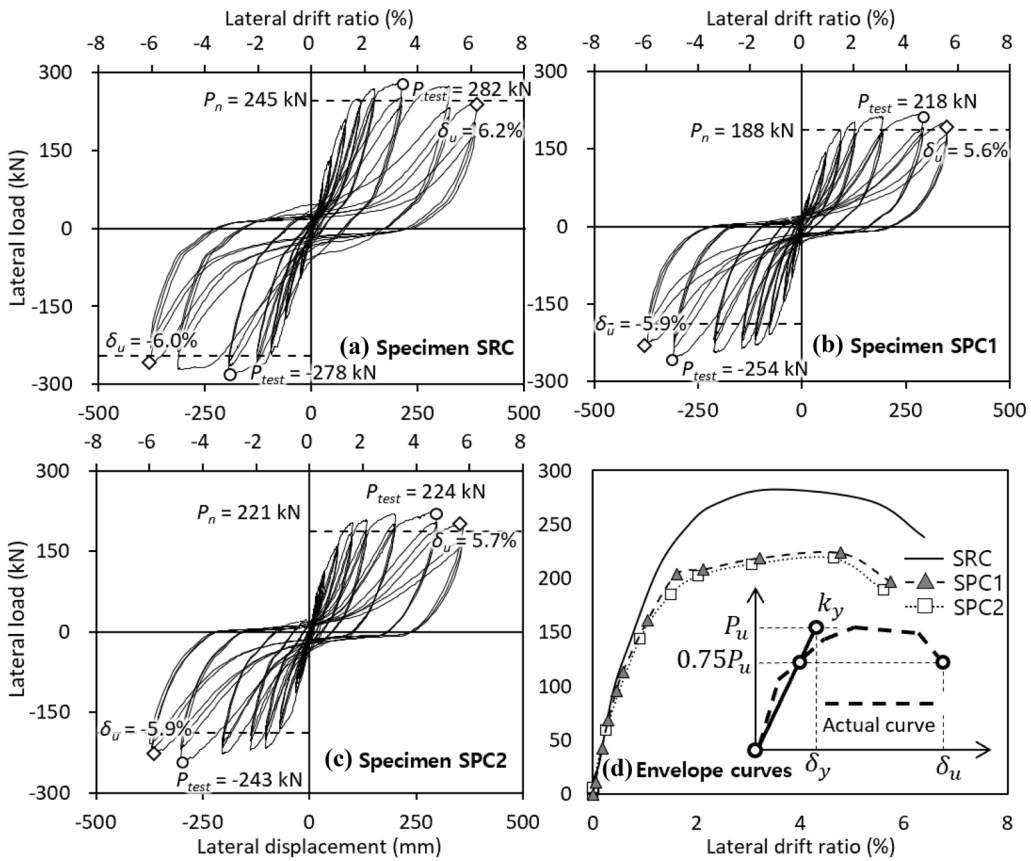

Fig. 15 Load–drift relations of specimens under cyclic lateral loading.

Table 3 Summary of test results and predictions.

Specimen	Load-carrying capacity			Deformation capacity			Stiffness (kN/mm)			
	Test results P_{test}[a]	Prediction P_n	P_{test} / P_n[a]	Yield drift ratio δ_y[a] (%)	Maximum drift ratio δ_u[a] (%)	Ductility μ[a]	k_y	k_i	k_s	k_s / k_i
GPC1	501	414	1.21	13.95	171.13	12.27	26.9	74.8	-	-
GPC1-AF	523	471	1.11	13.67	158.71	11.61	28.7	84.0	-	-
GPC2-AF	523	471	1.11	13.78	157.86	11.46	28.5	88.9	-	-
SRC	282|278	239	1.18|1.16	1.20|1.15	6.15|6.05	5.09|5.24	5.2	12.3	2.49	0.20
SPC1	218|254	188	1.17|1.35	1.28|1.06	5.59|5.95	4.35|5.58	4.23	12.0	2.00	0.17
SPC2	224|243	188	1.20|1.30	0.98|1.35	5.70|5.98	5.81|4.42	4.31	10.0	2.03	0.20

k_y = yield stiffness, k_i = initial stiffness, k_s = secant stiffness.

[a] Positive value | negative value.

increased, the bar-yielding occurred both within and outside the joint.

In the top bars of **SPC2** with the PC double beam–RC column connection (left-hand side of Fig. 16b), similar to **SRC** with the RC double beam–column connection, the strain of FC within the joint was significantly greater than the yield strain. However, the strain of FB outside the joint was smaller than that of **SRC** with the RC double beam–column connection, indicating that the damage was concentrated on the PC and CIP concrete interface of the connection and the plastic hinge length was limited due to the PC–RC interface (Fig. 14c). On the other hand, the strains in the bottom bars of **SRC** and **SPC2** (right-hand sides of Fig. 16a and b) were relatively smaller than those in the top bars. This tendency was also found in **SPC1**

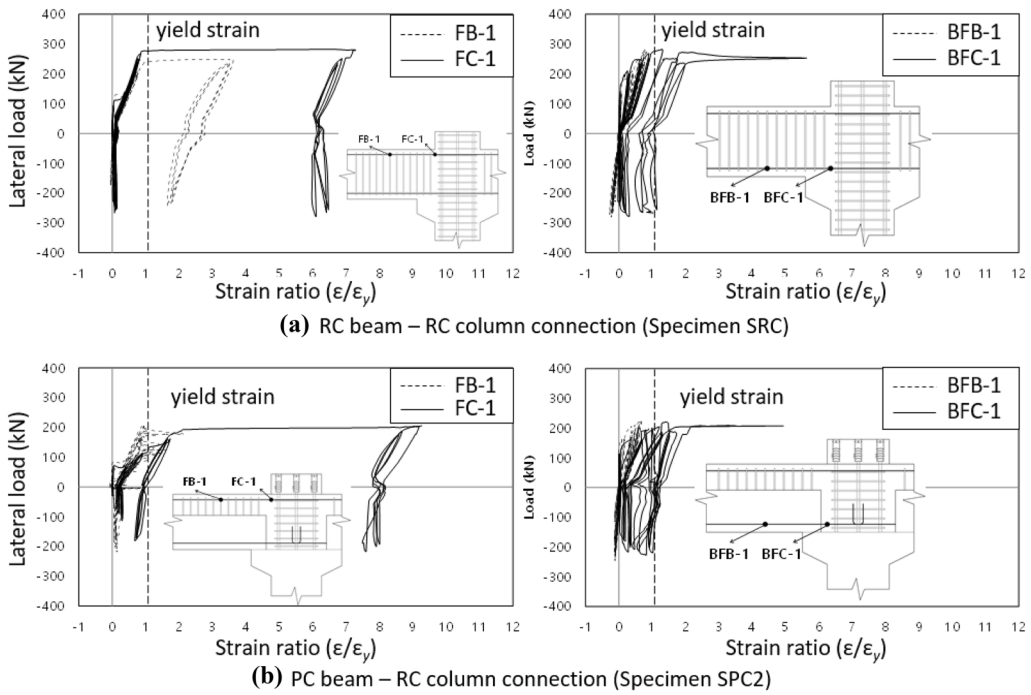

Fig. 16 Strain of flexural reinforcing bars in beams of specimens under cyclic lateral loading.

with the PC double beam–PC column connection (Fig. 14b).

5 Evaluation of Structural Performance

5.1 Load-Carrying Capacity and Deformation Capacity

The theoretical load-carrying capacity of the beam–column connection designed based on the strong-column-and-weak-beam concept can be predicted by assuming yielding of flexural rebars at the critical section, as follows (Im et al. 2010) (i.e., the interface between the PC beam and CIP concrete; Fig. 4b):

$$P_n = \left(P_{bp} + P_{bn}\right)\frac{l}{2h}, \tag{8a}$$

where P_n = the load-carrying capacity of the beam–column connection, P_{bp} and P_{bn} = vertical reactions at the beam supports, l = net beam length between the left and right beam hinge supports [= 4,760 mm], and h = net column height between the top and bottom hinges [= 3,060 mm]. The vertical reactions, P_{bp} and P_{bn}, were calculated by dividing the nominal flexural positive and negative moments, M_{bp} and M_{bn}, respectively, of the beam critical section by the shear span length $l_s = [l - (h_c - 2\,s)]/2$ (i.e., distance from the roller support to the critical section), where h_c = bracket depth and s = seating length of the PC beams. Thus, the load-carrying capacity of the PC double beam–column connection can be calculated as follows:

$$P_n = \left(M_{bp} + M_{bn}\right)\frac{l}{h}/(l - h_c + 2s) \qquad \text{for pc beam.} \tag{8b}$$

On the other hand, in the case of the RC double beam–column connection, the critical section crossed the side surface of the bracket. Thus, the load-carrying capacity for RC specimens can be calculated by excluding the seating length s of the PC beams, as follows (Im et al. 2010):

$$P_n = \left(M_{bp} + M_{bn}\right)\frac{l}{h}/(l - h_c) \qquad \text{for rc beam.} \tag{8c}$$

Table 3 and Fig. 15 show the theoretical load-carrying capacity P_n of the specimens calculated by Eq. (8). The flexural strength M_n of the beam critical section was calculated using the actual material strengths and rectangular concrete stress block of ACI 318 (ACI Committee 318, 2019) and KCI 2012 (Korea Concrete Institute 2012). Table 3 also presents the tested peak strength P_{test}, predicted strength P_n, strength ratio P_{test}/P_n, yield drift ratio δ_y, maximum drift ratio δ_u, and ductility $\mu = (\delta_u/\delta_y)$. As presented in Table 3 and Fig. 15, The P_{test}/P_n ratios of **SPC1** and **SPC2** with the PC double beam–column connection (1.17–1.35) were greater than 1.0, using Eq. (8b), which addresses the increased shear span length, l_s, due to the seating length s of the PC beams. This result indicates that the load-carrying capacity of the PC double beam–column connection can be conservatively

predicted by the theoretical load-carrying strength. On the other hand, by using Eq. (8c) for addressing the smaller shear span length l_s than that of the SPC specimens, the P_{test}/P_n value of **SRC** with the RC double beam–column connection (1.16–1.18) was close to or smaller than that of the SPC specimens. The overstrength may be due to the increasing plastic hinge length of the RC specimen with uniformly distributed cracks at the beam–column joint (Fig. 14a).

As shown in Table 3, **SPC1** and **SPC2** with the PC double beam–column connection exhibited maximum drift ratios of δ = 5.59%–5.98%, satisfying the requirement for the maximum drift ratios of beam–column connections (= 3.5%) in ACI 374.1–05 (ACI Committee 374, 2005 The displacement ductility ratios ranged from 4.35 to 5.81, which was close to that of **SRC** with the RC double beam–column connection (= 5.09–5.24), on average. This result indicates that the deformation capacity is identical to that for the RC double beam–column connection.

5.2 Energy Dissipation Capacity and Secant Stiffness

Figure 17 shows the variation in the hysteretic energy dissipation per cycle of the specimens with respect to the lateral drift ratio δ. The hysteretic energy dissipation E_D per cycle was calculated as the area enclosed by the third load cycle at each drift level. In Fig. 17a, the value of E_D for **SRC** with the RC double beam–column connection was smaller than those for **SPC1** and **SPC2** with the PC double beam–column connection before δ = 2.5%. However, after δ = 2.5%, the value of E_D for **SRC** with the RC double beam–column connection significantly increased and was greater than those for the PC double beam **SPC1** and **SPC2**. This was because **SRC** with more distributed cracks at the beam–column joint (Fig. 14a) dissipated energy faster than **SPC1** and **SPC2** with concentrated cracks at the PC-CIP concrete (Fig. 14b and c). However, by further increasing δ to 6.0%, the E_D of the PC double beam **SPC1** and **SPC2** was close to that of **SRC** with the RC double beam–column connection.

ACI 374.1-05 (ACI Committee 374 2005) recommends that at a drift level of no less than 3.5%, the energy dissipation ratio κ ($=E_D/E_{ep}$) by the third load cycle should be no less than 0.125, where E_{ep} denotes the energy dissipation per cycle attributable to the idealized elastic perfectly plastic behavior (Fig. 17b). As shown in Fig. 17b, regardless of the specimens, the energy dissipation capacity ratio κ was greater than 0.125 at a lateral drift ratio of 3.5%, satisfying the ACI 374.1–05 requirement.

ACI 374.1–05 also requires that, for the third load cycle at a drift level of no less than 3.5%, the secant stiffness for k_s ranging from −0.35% to + 0.35% should not be less than 0.05 times the initial stiffness k_i. Table 3 summarizes the initial stiffness k_i, secant stiffness k_s, and ratio k_s/k_i. In **SPC1** and **SPC2**, with the PC double beam–column connection, the k_s/k_i ratios were 0.17 to 0.20, which were greater than the ACI 374.1-05 requirement (= 0.05). The k_s/k_i ratios of **SPC1** and **SPC2** were not significantly inferior to that of **SRC** with the RC double beam–column connection (= 0.20).

5.3 Shear Strength of Beam–Column Joints

Table 4 presents the joint shear strength and demand, V_{jn} and V_{ju}, of the specimens evaluated using Eqs. (6) and (7), respectively. The joint shear strength V_{jn} of SRC with the conventional RC beam–column connection was calculated using γ = 1.2, and the effective joint shear area $A_j = 0.5(b_b + b_c)h_c$. The joint shear demand V_{ju} for **SRC** with RC double beam–column connection at the column face was calculated from Eq. (7) using $\alpha = 1.25$; $(C + T') = A_{st}f_y$ (A_{st} = total area of beam flexural bars at the critical section) and V_{col} = the tested peak strength P_{test}. On the

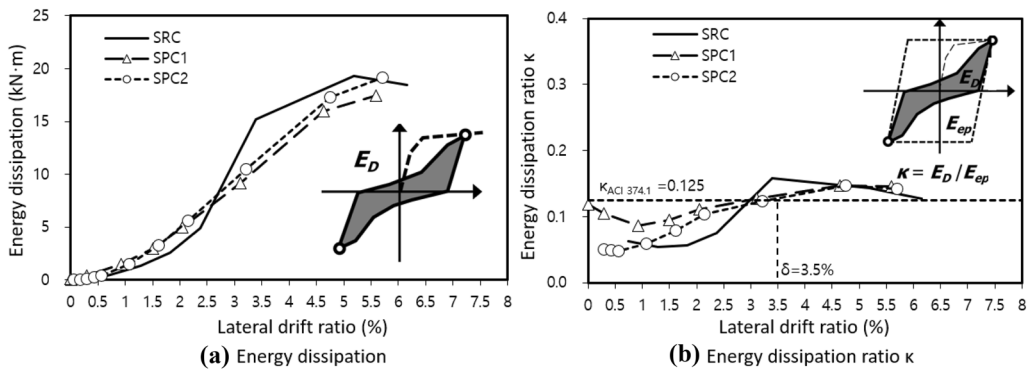

Fig. 17 Energy dissipation capacity of specimens under cyclic lateral loading.

Table 4 Joint shear strength of test specimens.

Specimen	f_c (MPa)	A_j (mm^2)	γ	V_{jn} (kN)	V_{ju} (kN)	V_{jn} / V_{ju}
SRC	40.5	298,200	1.2	2277	1216	1.87
SPC1	40.3	383,400	1.2	2921	1031	2.83
SPC2	40.3	383,400	1.2	2921	1025	2.85

f_c' = concrete compressive strength, A_j = effective joint shear area, γ = a coefficient addressing the confinement effect of beams framed into joint, V_{jn} = joint shear strength (Eq. 6), V_{ju} = joint shear demand (Eq. 7).

other hand, in the case of specimens with PC double beam–column connection (**SPC1** and **SPC2**), V_{jn} was $A_j = 0.5(b_b + b_c)(h_c\text{-}2\ s)$, considering the seating length $s = 150$ mm. The value of V_{ju} for **SPC1** and **SPC2** at the end of the PC double beam was calculated from Eq. (7) using $\alpha = 1.25$; $(C + T') = A_s f_y$; $V_{col} = P_{test}$.

Table 4 compares the joint shear demand V_{ju} and capacity V_{jn} of the specimens. For all specimens, V_{jn}/V_{ju} was greater than 1.0. This result agrees with the test results showing that joint shear failure did not occur (Fig. 14d–f).

6 Conclusion

Recently, as a new PC construction method for increasing economy and constructability, a PC double-beam system has been developed. This paper presents the test results of specimens with half-scaled beam–column connection with PC double beams under gravity loading or cyclic lateral loading, to investigate the integrity and structural capacity of the PC double beam–column connection. The major test parameters included the presence of a spliced column and the use of an additional flexural reinforcement at the beam–column joint.

The major findings of the gravity loading test are summarized as follows:

1. All specimens failed in flexural compression at the PC bracket–PC double-beam interface. The plastic hinge length l_p of the PC double beam was greater than the effective depth of beam d.
2. In the PC double beam under gravity load, the peak strength was 11%–21% greater than the predicted strength, by the current design code, which indicates that the composite action at the beam–column connection assumed for the PC members was valid for the PC double beam–column under gravity loading.
3. By using additional flexural rebars with a short anchorage length, the load-carrying capacity was increased at the initial loading, but gradually decreased due to the insufficient anchorage length. Thus, it is necessary to secure sufficient anchorage length considering a plastic hinge length.
4. The load-carrying capacity of specimens without the spliced PC column at the joint was comparable to that of specimens with the spliced PC column at the joint, which indicates that the spliced PC column at the joint had negligible effect on structural integrity.

The major findings of the cyclic lateral loading test are summarized as follows:

1. In the RC specimen, initial cracks occurred at the beam section adjacent to the end of the bracket, and gradually propagated toward the beams. In contrast, in the PC specimens, cracks were concentrated on the PC beam–CIP concrete.
2. In the RC specimen, bar-yielding occurred at the beam section adjacent to the end of the bracket and the yield penetration gradually propagated toward the beams. In contrast, in the PC specimens, yielding was concentrated on the top rebars across the RC–PC interface.
3. The peak strength of the PC specimens was 9%–22% smaller than that of the RC specimens. This was because (1) smaller number of longitudinal reinforcement was anchored into the topping concrete at the beam–column joint; (2) the shear span length l_s was increased by the seating length s due to the critical section at the PC beam–CIP concrete interface in PC specimens, and (3) the concentrated cracking and bar-yielding at the PC beam–CIP concrete interface did not increase the plastic hinge length. Nevertheless, the strength ratios to the predictions by the current design code were greater than 1.0 in the PC specimens.
4. The seismic performance of specimens without the PC column at the joint was comparable to that of specimens with the PC column at the joint, indicating that the RC column had a negligible effect on structural integrity.
5. The deformation capacity, energy dissipation capacity, secant stiffness, and shear strength of the PC specimens were comparable to those of a conventional RC specimen and satisfied the acceptance

criteria of moment frame in the ACI 374.1–05 (ACI Committee 374 2005) provision.

This study focused on the interior joints of PC double beam–column connection. However, an exterior joint of PC double beam–column connection, which is common in actual structure and is known to be more vulnerable to seismic excitations, requires careful design procedure and reinforcement arrangement, similar to those carried out for other new construction methods (Chalioris and Bantilas 2017; Ghayeb et al. 2017). Thus, further study is necessary to investigate the exterior joint of PC double beam–column connection.

Acknowledgements
This research was carried out with the support of the Researcher Support Program (NRF-2018R1A2B6007559) hosted by the National Research Foundation of Korea (NRF), and this work (Grants No. C0353376) was supported by Business for Cooperative R&D between Industry, Academy, and Research Institute funded Korea Small and Medium Business Administration in 2015.

Authors' information
J. W. Baek is an Assistant Professor in the Department of Civil Engineering and Environmental Sciences at Korea Military Academy, Seoul, South Korea. He received his BE, MS, and PhD in the Department of Architecture & Architectural Engineering at Seoul National University. His research interests include design and behavior of shear wall under seismic or blast loads.

S. M. Kang is an Associate Professor in the School of Architecture at Soongsil University, Seoul, South Korea. He received his BE, MS, and PhD in the Department of Architecture & Architectural Engineering at Seoul National University. His research interests include earthquake design of building structures (Corresponding Author).

T. H. Kim is a general manager in Architecture Engineering & Research Team at Daelim Industrial Company. He received his PhD in the Department of Architectural Engineering at SungKyunKwan University. His research interests include the design of precast concrete structures.

J. Y. Kim is an Assistant Manager in SENVEX Co. Ltd, Seoul, Korea. He received his BE, MS in the Department of Architectural Engineering at Chungbuk National University. His research interests include development of beam–column joint to secure seismic performance.

Authors' contributions
The first author, J. W. Baek, analyzed the data and wrote this manuscript. The corresponding author, S. M. Kang, planned and supervised the project, and reviewed this manuscript. T. H. Kim designed the PC double-beam system, and J.Y. Kim performed the experiments and provided the experimental data. All authors read and approved the final manuscript.

Availability of data and materials
Some data analyzed in this study are available in the master's course thesis of J.Y. Kim at Chungbuk National University in 2018.

Competing interests
The authors declare that they have no competing interests.

Author details
[1] Department of Civil Engineering and Environmental Sciences, Korea Military Academy, 570, Hwarang-ro, Nowon-gu, Seoul 01805, Republic of Korea. [2] School of Architecture, Soongsil University, 369 Sangdo-ro, Dongjak-Gu, Seoul 06978, Republic of Korea. [3] Architecture Engineering and Research Team, Daelim Industrial Company, 36, Jong-ro 1 gil, Jongno-gu, Seoul 03152, Republic of Korea. [4] SENVEX Co. Ltd, 6 Beodeunaru-ro 19-gil, Yeongdeungpo-Gu, Seoul 07226, Republic of Korea.

Received: 4 April 2020 Accepted: 8 September 2020
Published online: 10 December 2020

References

ACI Committee 318. (2014). *Building Code Requirements for Structural Concrete (ACI 318–14) and Commentary*. Farmington Hills, MI: American Concrete Institute.
ACI Committee 318. (2019). *Building Code Requirements for Structural Concrete (ACI 318–19): An ACI Standard: Commentary on Building Code Requirements for Structural Concrete (ACI 318R-19)*. Farmington Hills: American Concrete Institute.
ACI Committee 374. (2005). *Acceptance Criteria for Moment Frames Based on Structural Testing and Commentary: An ACI Standard*. Farmington Hills, MI: American Concrete Institute.
Bae, S., & Bayrak, O. (2008). Plastic hinge length of reinforced concrete columns. *ACI Structural Journal, 105*(3), 290.
Chalioris, C. E., & Bantilas, K. E. (2017). Shear strength of reinforced concrete beam-column joints with crossed inclined bars. *Engineering Structures, 140,* 241–255.
Corley, W. (1966). Rotational capacity of reinforced concrete beams. *Journal of the Structural Division, 92*(5), 121–146.
Dalalbashi, A., Eslami, A., & Ronagh, H. R. (2012). Plastic hinge relocation in RC joints as an alternative method of retrofitting using FRP. *Composite Structures, 94*(8), 2433–2439.
Eom, T.-S., Park, H.-G., Hwang, H.-J., & Kang, S.-M. (2015). Plastic hinge relocation methods for emulative pc beam-column connections. *Journal of Structural Engineering, 142*(2), 04015111.
Fenwick, R. C., & Irvine, H. M. (1977). *Reinforced concrete beam-column joints for seismic loading: Department of Civil Engineering*. Auckland: University of Auckland.
Ghayeb, H. H., Razak, H. A., & Sulong, N. R. (2017). Development and testing of hybrid precast concrete beam-to-column connections under cyclic loading. *Construction and Building Materials, 151,* 258–278.
Girhammar, U. A., & Pajari, M. (2008). Tests and analysis on shear strength of composite slabs of hollow core units and concrete topping. *Construction and Building Materials, 22*(8), 1708–1722.
Han, M.-Y., Jin, K.-S., & Choi, S.-H. (2010). Flexural test for a monolithic holed web prestressed concrete (HWPC) girder. *International Journal of Concrete Structures and Materials, 4*(2), 77–87.
Hassan, T., & Rizkalla, S. (2002). Flexural strengthening of prestressed bridge slabs with FRP systems. *PCI journal, 47*(1), 76–93.
Hirosawa, M. (1977). Strength and ductility of reinforced concrete members in Japanese. *Report of the Building Research Institute*(76), 1967–1974.
Hsu, C.-T.T. (1989). T-shaped reinforced concrete members under biaxial bending and axial compression. *Structural Journal, 86*(4), 460–468.
Im, H.-J., Park, H.-G., Eom, T.-S., & Kang, S.-M. (2010). Earthquake resistance of beam-column connection of precast concrete U-shaped shell construction. *Journal of the Korea Concrete Institute, 22*(6), 741–751.
Joh, O., Goto, Y., & Shibata, T. (1991). Influence of transverse joint and beam reinforcement and relocation of plastic hinge region on beam column joint stiffness deterioration. *Special Publication, 123,* 187–224.
Joint ACI-ASCE Committee 352. (2002). *Recommendations for design of beam-column connections in monolithic reinforced concrete structures (ACI 352R-02)*. Farmington Hills: American Concrete Institute.
Juette, B. (1996). *Moving beam plastic hinges in reinforced concrete frames using headed reinforcement bars.* MS thesis, Univ. at Karlsruhe, Germany.
Kim, T.-H., Seong, D.-J., & Shin, H. M. (2012). Seismic performance assessment of hollow reinforced concrete and prestressed concrete bridge columns. *International Journal of Concrete Structures and Materials, 6*(3), 165–176.
Korea Concrete Institute. (2012). *Concrete design code and commentary*. Korea: Kimoondang.
Lee, J. D., Yoon, J. K., & Kang, T.H.-K. (2016). Combined half precast concrete slab and post-tensioned slab topping system for basement parking structures. *Journal of Structural Integrity and Maintenance, 1*(1), 1–9.

Masi, A., Santarsiero, G., & Nigro, D. (2013). Cyclic tests on external RC beam-column joints: role of seismic design level and axial load value on the ultimate capacity. *Journal of Earthquake Engineering, 17*(1), 110–136.
Meinheit, D. F., & Jirsa, J. O. (1977). Shear strength of reinforced concrete beam-column joints. *Department of Civil Engineering, Structures Research Laboratory, University of Texas at Austin, Austin, TX*(77–1), 291. https://doi.org/10.14359/51685433
Panagiotakos, T. B., & Fardis, M. N. (2001). Deformations of reinforced concrete members at yielding and ultimate. *Structural Journal, 98*(2), 135–148.
Park, M.-K., Lee, D. H., Han, S.-J., & Kim, K. S. (2019). Web-shear capacity of thick precast prestressed hollow-core slab units produced by extrusion method. *International Journal of Concrete Structures and Materials, 13*(1), 7.
Park, R. (1988). *Ductility Evaluation from Laboratory and Analytical Testing.* Paper presented at the the 9th World Conference on Earthquake Engineering, Tokyo-Kyoto, Japan.
Paulay, T., & Priestley, M. (1992). *Seismic design of reinforced concrete and masonry buildings*. New York: Wiley.
Paulay, T., & Priestley, M. N. (1992). Seismic design of reinforced concrete and masonry buildings.
Ren, W., Sneed, L. H., Yang, Y., & He, R. (2015). Numerical simulation of prestressed precast concrete bridge deck panels using damage plasticity model. *International Journal of Concrete Structures and Materials, 9*(1), 45–54.
Yamamoto, Y., Nagai, O., & Maruta, M. (2008). Structure performance of hinge relocated RC slab-wall frame. *Proc. Jpn. Concr. Inst, 30*(3), 397–402.

Publisher's Note